Computational Fluid Dynamics-Based Multiobjective Optimization for Catalyst Design

Shueh-Hen Cheng,[†] Hsuan Chang,*[,‡] Yih-Hang Chen,[‡] Hsi-Jen Chen,[‡] Yung-Kang Chao,[‡] and Yu-Hsiang Liao[‡]

Department of Chemical and Materials Engineering, Tunghai University, Taichung, 40704, Taiwan, Energy and Opto-Electronic Materials Research Center, Department of Chemical and Materials Engineering, Tamkang University, Taipei County, 25137, Taiwan

For an industrial secondary methane steam reformer with regular packing, catalyst design is accomplished by an integrated optimization approach, which includes the design of experiment, computational fluid dynamics (CFD) simulation, a response surface method, and a genetic algorithm, for multiobjective optimization. Both spherical and cylindrical catalysts are studied. The reactor performance considered for the catalyst design includes the pressure drop and hydrogen production, which constitute the binary objective functions for optimization. The optimal solutions reveal that a large pore diameter, near 1 μm, should be adopted for spherical catalysts. For cylindrical catalysts, the optimal design suggests the use of a 1-big-hole shape with a larger particle and pore size, 10−13 mm and near 1 μm, or a 4-hole shape with a smaller particle size of 6−8 mm.

Introduction

The packed bed reactor (PBR) is the main reactor type applied in industrial heterogeneously catalyzed gas-phase reactions. Catalyst design is an important subject to PBR because it affects the reactor performance in many aspects, including the pressure drop, reaction extent, product distribution, etc.[1] The advances in scientific computing to simulate the flow field and the introduction of chemical reactions into commercial computational fluid dynamics (CFD) packages have put forward rapid progress in the application of CFD in chemical reaction engineering. The methodology and development of 3D CFD modeling for PBR, including issues of the turbulent model, reactor geometry, contact point treatment, boundary-layer treatment, and boundary conditions, can be found in the comprehensive in-depth review by Dixon et al.[2] Most of the published CFD studies of PBR are on the fluid flow and heat transfer in the reactors.[3−7] Recently, CFD simulation taking into account intraparticle diffusion, heat transfer, and chemical reactions has been reported for a steam reforming reactor.[8] For catalyst design, the comparison of the heat transfer performance under specified reaction thermal effects for different cylindrical pellet designs has been investigated using CFD.[9−11]

Because of the intensive computational resources needed, it is impractical to implement an optimization study with CFD simulation. While tackling the optimization problems for the systems which must be described with complex mathematical models, the genetic algorithm,[12] which is a stochastic searching method, is a feasible approach. The genetic algorithm has been broadly applied for multiobjective optimization, which provides multiple optimal solutions with trade-offs.[13−16] For effectively utilizing CFD analysis tools in optimization, an integrated approach, which couples the CFD model with a genetic algorithm, a design of experiment, and a response surface method, has been proposed and applied for the multiobjective optimization of the turbo pump and compressor blade.[17]

Although many studies have focused on the CFD simulation methodology for PBR and the application of CFD analysis for PBR catalyst design has gained considerable attention, catalyst design optimization based on CFD simulation has not been reported. In this work, the integrated optimization approach[17] is implemented for the multiobjective optimization of catalyst design for PBR. For a catalytic methane steam reforming PBR, optimization studies are presented for both spherical catalysts and cylindrical catalysts.

CFD Simulation

The secondary reformer in an industrial ammonia plant using a Ni based catalyst is adopted for this study.[18] The secondary reformer is for further converting methane from the primary reformer and provides proper ratio of synthesis gas to nitrogen by controlling the air flow rate. The secondary reformer is normally operated adiabatically with energy supplied by the partial oxidation of methane. The inlet gas to the catalyst bed comes from a combustion zone, and the gas conditions[18] and the reactions are listed in Table 1. The reaction kinetics given by De Groote and Froment[19] and Xu and Froment[20] are used.

The catalyst packing in the reactor is a key issue for PBR CFD simulation. Many researchers have proposed different reactor structures, as have been reviewed in Dixon et al.[2] The goal is to define the catalyst packing structure, which is representative of realistic conditions but not too expensive to compute. On the basis of experimental study and the theoretical packing method, representative reactor structures for spherical or equilateral cylindrical catalysts with a tube-to-particle diameter ratio (N) of 4 have been created[9,21] in the literature. The studies[9,21] have also concluded that a 120° wall segment gives good agreement with the full bed simulation. These configurations, depicted in Figure 1, are used in this work. For the optimization studies, the variations of the equilateral cylindrical catalysts are those discussed in the literature, i.e., solid (0-hole), 1-hole, 1-big-hole, 3-hole, 4-hole, and 4-small-hole.[11] The diameter of a standard hole is 28.66% of the cylinder diameter, and the diameters of a big hole and a small hole are 2 times and 2.5 times that of a standard hole, respectively. These

* To whom correspondence should be addressed. Tel.: +886 226232094. Fax: +886 226209887. E-mail: nhchang@mail.tku.edu.tw.
[†] Tunghai University.
[‡] Tamkang University.

10.1021/ie1001839
Published on Web 05/06/2010

Table 1. Reactor Inlet Gas Conditions and Reactions

inlet gas conditions	
pressure (bar)	24.52
temperature (K)	1044.00
composition (mol %)	
CH_4	2.25
H_2O	60.87
CO	3.85
H_2	17.96
CO_2	4.49
O_2	2.24
N_2	8.34

reactions		
$CH_4 + 2O_2 \xrightarrow{R_1} CO_2 + 2H_2O$	(17)	$\Delta H_{rxn,1} = -802.2$ kJ/mol
$CH_4 + H_2O \overset{R_2}{\leftrightarrow} CO + 3H_2$	(18)	$\Delta H_{rxn,2} = 206.1$ kJ/mol
$CO + H_2O \overset{R_3}{\leftrightarrow} H_2 + CO_2$	(19)	$\Delta H_{rxn,3} = -41.1$ kJ/mol
$CH_4 + 2H_2O \overset{R_4}{\leftrightarrow} CO_2 + 4H_2$	(20)	$\Delta H_{rxn,4} = 165.0$ kJ/mol

variations of the cylindrical catalysts do not alter the packing structure of the simulated bed.

The simulation is carried out by the commercial CFD software FLUENT v. 6.3.26 with the geometries created by GAMBIT v. 2.2.30. The turbulent flow is simulated using the renormalization group (RNG) k-€ model with enhanced wall treatment.[11,22] To avoid the generation of skewed cells, nodes are first created on the surfaces near the contact points, with the node distances gradually increased in the direction away from the contact points. Unstructured tetrahedral cells are then generated on the basis of these nodes. For the reactor wall, prism layers with gradually increased thickness are used. A grid independent analysis has been conducted by comparing the velocity profiles

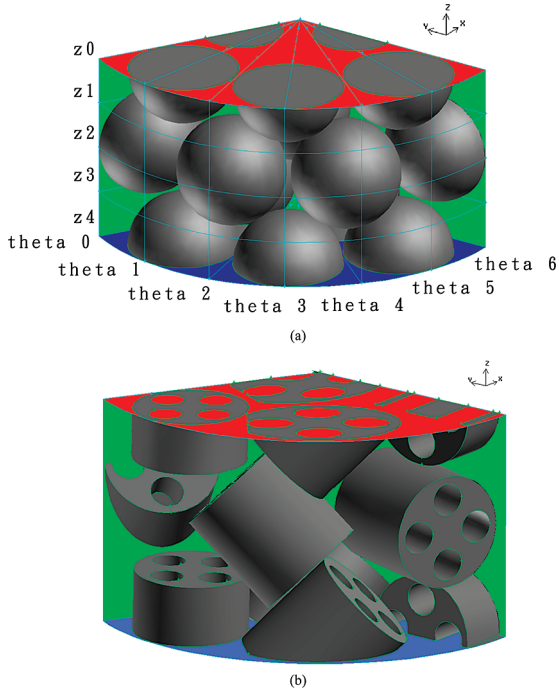

Figure 1. Packing structures for spherical (a) and cylindrical (b) catalysts.

and the dimensionless distance parameter ($y^+ < 1$). The smallest node distance and the first prism layer thickness used are $0.015d_P$ and $2.5 \times 10^{-4}d_P$.

The catalysts are treated as a porous media type of fluid in FLUENT, which is solved as a normal fluid phase except that a momentum source term is added to account for the viscous loss and the inertial loss inside the porous media.[22] Hence, the heat transfer, species diffusion and chemical reactions within the catalyst particles can be solved. Although the catalyst particle is defined as a porous medium, because of the small pore size, the fluid convection inside the particle is trivial. User-defined codes are provided to FLUENT for the calculation of reaction rates and properties, such as the component diffusivities inside the catalyst particles to consider the Kundsen and molecular diffusions.

The governing equations for simulating the packed bed reactor with a catalyst particle being treated as a porous media fluid are elucidated as follows. The continuity equation and the species mass balance equation are given in eqs 1 and 2. In eq 2, the chemical reaction source term evaluated using eq 3 applies to the catalyst particle only. The term must be taken into account as eq 3. The estimation of mass diffusion by eq 4 includes the molecular and turbulent diffusion. The turbulent Schmidt number (Sc_t) is set to be 0.7.

$$\nabla(\rho\vec{v}) = 0 \tag{1}$$

$$\nabla(\rho\vec{v}y_i) = -\nabla\vec{j}_i + R_i \tag{2}$$

$$R_i = M_{wi}\sum_{r=1}^{N_R}\hat{R}_{i,r} \tag{3}$$

$$\vec{j}_i = -\left(\rho D_i + \frac{\mu_t}{Sc_t}\right)\nabla y_i \tag{4}$$

The momentum balance equation is given in eq 5 with a momentum source term ($\vec{F}$). For the bulk gas, the source term is zero. For the catalyst particle, eq 6 is used to account for the viscous loss. The stress tensor is defined by eq 7, where the turbulent viscosity (μ_t) is determined by the RNG k-€ turbulent model. The details of the turbulent model can be found in the literature.[22]

$$\nabla(\rho\vec{v}\vec{v}) = -\nabla P + \nabla\bar{\bar{\tau}} + \vec{F} \tag{5}$$

$$\vec{F} = -\frac{\mu}{\alpha}\vec{v} \tag{6}$$

$$\bar{\bar{\tau}} = (\mu + \mu_t)\left[(\nabla\vec{v} + \nabla\vec{v}T) - \frac{2}{3}\nabla\vec{v}I\right] \tag{7}$$

The energy balance equation in eq 8 includes a source term of the chemical reaction heat effect as defined in eq 9. The turbulent Prandtl number (Pr_t) is set to be 0.85. The thermal conductivity in the porous medium is computed as the volume average of the gas conductivity and the solid conductivity.

$$\nabla\left(\vec{v}\left(\rho\left(\sum_j y_j h_j + \frac{v^2}{2}\right) + P\right)\right) = \nabla\left(\left(k_c + \frac{C_p\mu_t}{Pr_t}\right)\nabla T - \sum_j h_j\vec{J}_j + (\bar{\bar{\tau}}\vec{v})\right) + S_h \tag{8}$$

$$S_h = -\sum_i \frac{h_i^o}{M_{w,i}} R_i \tag{9}$$

The reactor segments shown in Figure 1 are simulated on the basis of the "virtual stacking" and "axially periodic" ideas.[6,9] To obtain results which can represent a typical section of the PBR, the isothermal simulation of the fluid flow is implemented first and in such a way that the profiles of the outlet boundary from the previous run are used as the profiles of the inlet boundary of the subsequent run. The process is repeated until no significant differences can be found in the profiles of the inlet and outlet boundaries.

The boundary conditions are the constant inlet mass flux for the inlet (top) fluid region, pressure outlet for the outlet (bottom) fluid region, symmetry for the inlet and outlet solid (catalyst) regions, symmetry for the two segment side boundary faces, and adiabatic with a no slip condition for the reactor wall. The catalyst-fluid interface is set as an interior surface instead of a solid wall. A comparison of the fluid flow simulations for the two types of the catalyst surface setting shows insignificant differences in the pressure and velocity profiles as well as the y^+ values. The setting of the interior surface allows transfers between the fluid and the catalysts to be simulated without using user-defined codes.

The SIMPLE pressure−velocity coupling algorithm with the first order upwind scheme is used for the simulation. Under relaxation factors used for solving variables ranging between 0.2 and 0.6. The convergence of the simulation is based on the residuals for governing equations and the reaction rates. The gas properties, such as viscosity, thermal conductivity, and diffusivity, are calculated using user-defined codes. The solid properties are based on those of alumina, and the porosity of the catalyst particle is assumed to be 0.43.[1]

Comparison of the pressure drop results from the experiment, CFD simulation, and Ergun correlation[23] has been commonly adopted for examining the CFD models. For example, Calis et al.[24] reported the comparisons for packed reactors of spherical catalysts with a tube-to-particle diameter ratio (N) of 1.0 to 2.0. Their analysis concludes that the Ergun correlation overpredicts the experimental results by an average of 80%, but the results from CFD simulations and experiments are close. For the cases simulated in our study, the average deviations of the pressure drop predictions by Ergun correlation from that by CFD simulation are 45% for the spherical catalysts and 10% for the cylindrical catalysts.

Multiobjective Optimization

The performance of catalysts can be evaluated by many factors, such as the reactor exit composition, approach to equilibrium, activity, or active volume of the catalyst.[1] Some studies of catalyst design focused on the effectiveness factor and pressure drop[25] or active surface area per unit volume, bed voidage, pressure drop, and transport properties.[26] A catalyst design study using CFD simulation has been presented for the investigation of catalyst thermal performance.[11]

In this optimization study, the reactor performances investigated are the pressure drop and the hydrogen production rate. They are defined as the following two objective functions:

$$f_1 = \frac{\Delta P/L}{(\Delta P/L)_{ref}} \tag{10}$$

$$f_2 = 1 - \frac{3R_2 + R_3 + 4R_4}{R_{H_2,ref}} \tag{11}$$

The hydrogen production rate is evaluated using the reaction rates R_2, R_3, and R_4, as given in the numerator of the second term on the right-hand side of eq 11. Both functions are normalized using appropriate reference values. By defining f_2 as eq 11, both objective functions are to be minimized. The design variables of the multiobjective optimization problems are the catalyst particle diameter (d_P) and catalyst pore diameter (d_{pore}) for the spherical case and the catalyst particle diameter (d_P), catalyst pore diameter (d_{pore}), and catalyst shape for the cylindrical case. The ranges of the design variables are based on realistic industrial applications:[27] 6−17 mm for d_P and 0.01−1 μm for d_{pore} and the previously mentioned six types of cylindrical catalyst shapes.

The optimization is subject to the inlet gas conditions given in Table 1 and a constant inlet gas mass flux of 11.7 kg/m^2 s.

Because the reactor performance must be obtained by the complex CFD simulation, the integrated optimization approach[17] is adopted for this work. The approach implements the multiobjective optimization on a surrogate model, which represents the relationships between the objective functions and the design variables. The multiple nondominated, Pareto-optimal, or compromised solutions are then obtained by applying the genetic algorithm on the surrogate model. The response surface methodology[28] is used to generate the surrogate model, which approximates the CFD simulation with low-order polynomial functions by regression on selected design points. The design points are determined systematically by a method of design of experiment. The expensive CFD simulation can hence be conducted for those design points only. The flow diagram of the integrated approach is depicted in Figure 2.

In this work, the Latin hypercube design (LHD) method,[29] which is a popular choice of experimental design method when computer simulation is used to study a physical process and is a favorable space-filling design method, is first employed to determine the design points for CFD simulation. To apply the LHD method, the number of data points needed must be specified first. It is determined by the number of design variables and the order of the polynomial function for the response surface

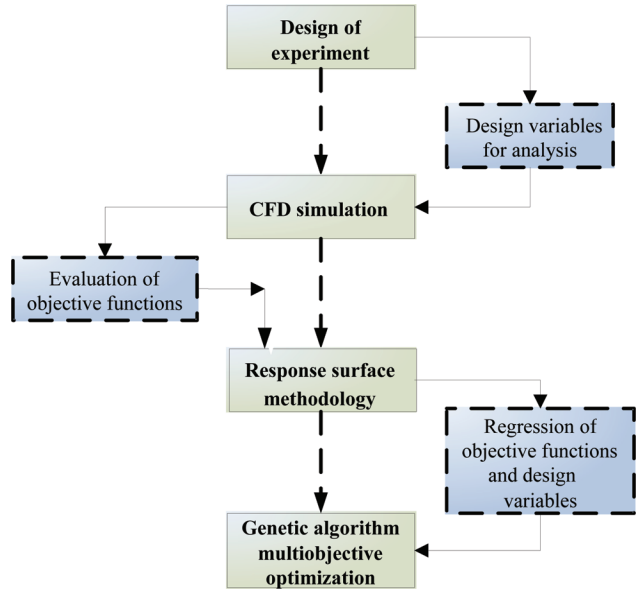

Figure 2. Integrated optimization approach.

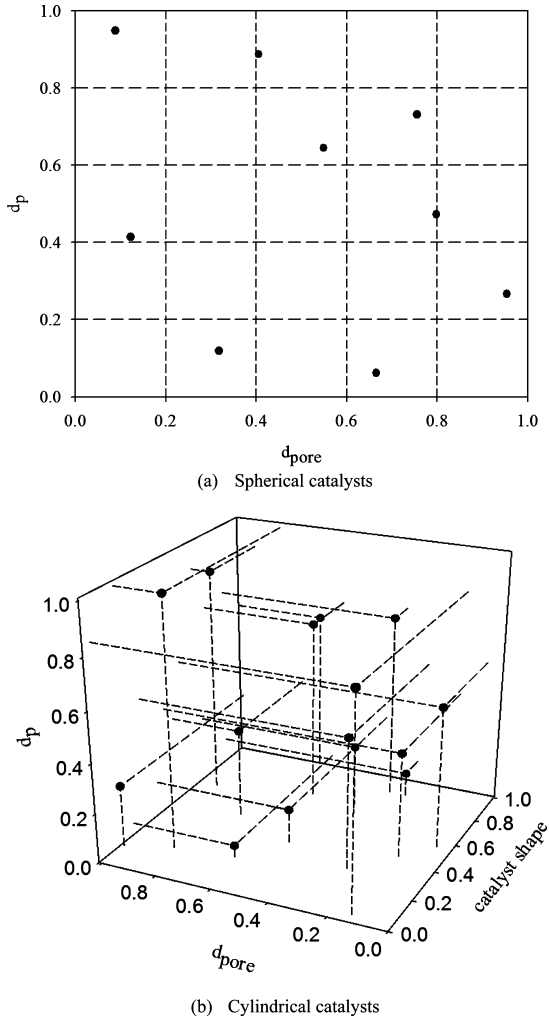

(a) Spherical catalysts

(b) Cylindrical catalysts

Figure 3. Design points determined by Latin hypercube design.

regression. The study adopts the widely used second-order polynomial function. For d variables, the function can be written as

$$f = \beta_0 + \sum_{i=1}^{d} \beta_i x_i + \sum_{i=1}^{d} \beta_{ii} x_i^2 + \sum_{j=2}^{d} \sum_{i=1}^{j-1} \beta_{ij} x_i x_j + \varepsilon \tag{12}$$

where f is the objective function, x represents the design variables, β represents the regression coefficients, and ε denotes the total error, which is the difference between the simulated and the estimated response value.

The spherical and cylindrical catalyst design problems involve two and three design variables, respectively. The number of design points used is 50% overdetermined for better performance of the response surface model.[30] The design points for the spherical and cylindrical catalyst problems are shown in Figure 3 and Table 2. Note that the variables are converted into values in the range of 0−1 in Figure 3.

The CFD simulations are then conducted for these design points, and the results are summarized in Tables 3 and 4, including the Reynolds number, pressure drop, and reaction rates. The Reynolds number, *Re*, is based on the hydraulic diameter and the interstitial velocity.

On the basis of the CFD simulation results, the coefficients of the second-order polynomial equations are determined using the multiple linear regression[28] method and the method of least-squares.

Table 2. Design Points Determined by Latin Hypercube Design

case no.	d_P (mm)	d_{pore} (μm)	shape
sphere-01	9	0.810	
sphere-02	10	0.018	
sphere-03	13	0.125	
sphere-04	16	0.065	
sphere-05	11	0.395	
sphere-06	6	0.214	
sphere-07	7	0.043	
sphere-08	17	0.015	
sphere-09	14	0.325	
cylinder-01	16	0.018	solid
cylinder-02	7	0.037	4-hole
cylinder-03	9	0.065	4-small-hole
cylinder-04	12	0.012	3-hole
cylinder-05	14	0.147	4-small-hole
cylinder-06	13	0.220	4-hole
cylinder-07	12	0.033	1-hole
cylinder-08	11	0.019	1-big-hole
cylinder-09	6	0.174	1-hole
cylinder-10	10	0.307	1-big-hole
cylinder-11	9	0.938	solid
cylinder-12	7	0.101	1-big-hole
cylinder-13	16	0.718	3-hole
cylinder-14	14	0.048	4-hole
cylinder-15	17	0.455	1-hole

For spherical case, with $(\Delta P/L)_{ref} = 45.1$ kPa/m and $R_{H_2,ref} = 3.6$ kmol/(kg cat s), the results are

$$f_1 = 1.92 + 3.52 \times 10^5 d_{pore} - 205.5 d_p + 3.3 \times 10^{11} d_{pore}^2 + 6376 d_p^2 - 1.11 \times 10^7 d_{pore} d_p \tag{13}$$

$$f_2 = -0.17 - 9.42 \times 10^5 d_{pore} + 97 d_p + 3.95 \times 10^{11} d_{pore}^2 - 2770 d_p^2 + 3.8 \times 10^7 d_{pore} d_p \tag{14}$$

For the cylindrical case, the variable of catalyst shape is treated as a classification variable. With $(\Delta P/L)_{ref} = 80$ kPa/m and $R_{H_2,ref} = 4.6$ kmol/(kg cat s), the results are

$$f_1 = 0.22 - 0.04 d_{pore} + \alpha_1 d_p - 0.83 d_{pore} d_p \tag{15}$$

$$f_2 = 0.11 + 0.74 d_{pore} + \alpha_2 d_p - 0.45 d_{pore} d_p \tag{16}$$

The coefficients α_1 and α_2 have different values corresponding to different shapes of the cylindrical catalysts. For the solid, 1-hole, 1-big-hole, 3-hole, 4-small-hole, and 4-hole shapes, the values of α_1 are 0.39, 0.84, 0.32, 0.68, 0.64, and 0.48 and the values of α_2 are 0.23, 0.21, 0.02, 0.1, 0.2, and −0.01.

Several response surfaces are given in Figure 4. The R^2 and R_{adj}^2 of the regression results for the spherical and cylindrical cases are higher than 99.7 and 99.3% and 99.8 and 96.7%, respectively.

With the availability of the surrogate model, the widely adopted genetic algorithm method, NSGA-II,[31] is employed for obtaining the optimal solutions. NSGA-II is one of the most efficient multiobjective evolutionary algorithms using the elitist approach. Its particular fitness assignment scheme consists of sorting the population in different fronts using the nondomination order relation. Then, to form the next generation, the algorithm combines the current population and its offspring generated with the crossover and mutation operations. Finally, the best individuals in terms of nondominance and diversity are chosen. Using NSGA-II requires the specification of six parameters, including the population size, number of generations for iteration, probability and distribution indexes for crossover operation, and probability and distribution indexes for mutation operation. The determination of these parameters is normally done by varying their values and examining the effects on the optimal solutions. For both spherical and cylindrical cases, the values of these parameters used are 50, 200, 0.85, 20, 0.1, and 20.

Table 3. CFD Simulation Results for Spherical Catalyst Design Points

Case No.	*Re*	$\Delta P/L$ (Pa/m)	R_1 (10^{-3} kmol/m^3 s)	R_2 (kmol/m^3 s)	R_3 (kmol/m^3 s)	R_4 (kmol/m^3 s)
sphere-01	14509	26246	3.1708	0.3291	0.9960	0.1696
sphere-02	16121	23050	2.5593	0.2226	0.6626	0.1112
sphere-03	20958	16538	2.4363	0.1965	0.5808	0.9849
sphere-04	25794	12855	2.2748	0.1585	0.4737	0.0791
sphere-05	17733	20378	2.7711	0.2573	0.7550	0.1304
sphere-06	9673	44045	3.2249	0.3730	1.0879	0.1939
sphere-07	11285	36168	2.8389	0.2956	0.8653	0.1497
sphere-08	27406	11926	2.2506	0.1462	0.4407	0.0728
sphere-09	22570	15104	2.5113	0.2042	0.5981	0.1026

Results and Discussion

Effects of Catalyst Design Variables. For the simulated design points listed in Table 2, some discussions on the effects of design variables can be made on the basis of the results listed in Tables 3 and 4 as well as Figures 5 and 6. For the spherical catalysts, the pressure drop decreases with an increase of the Reynolds number, and the change follows a smooth curve. For the cylindrical catalysts, due to the shape variation, although the general trend is the same, the data are more scattered. The effect of the catalyst pore size on the intraparticle mass diffusion

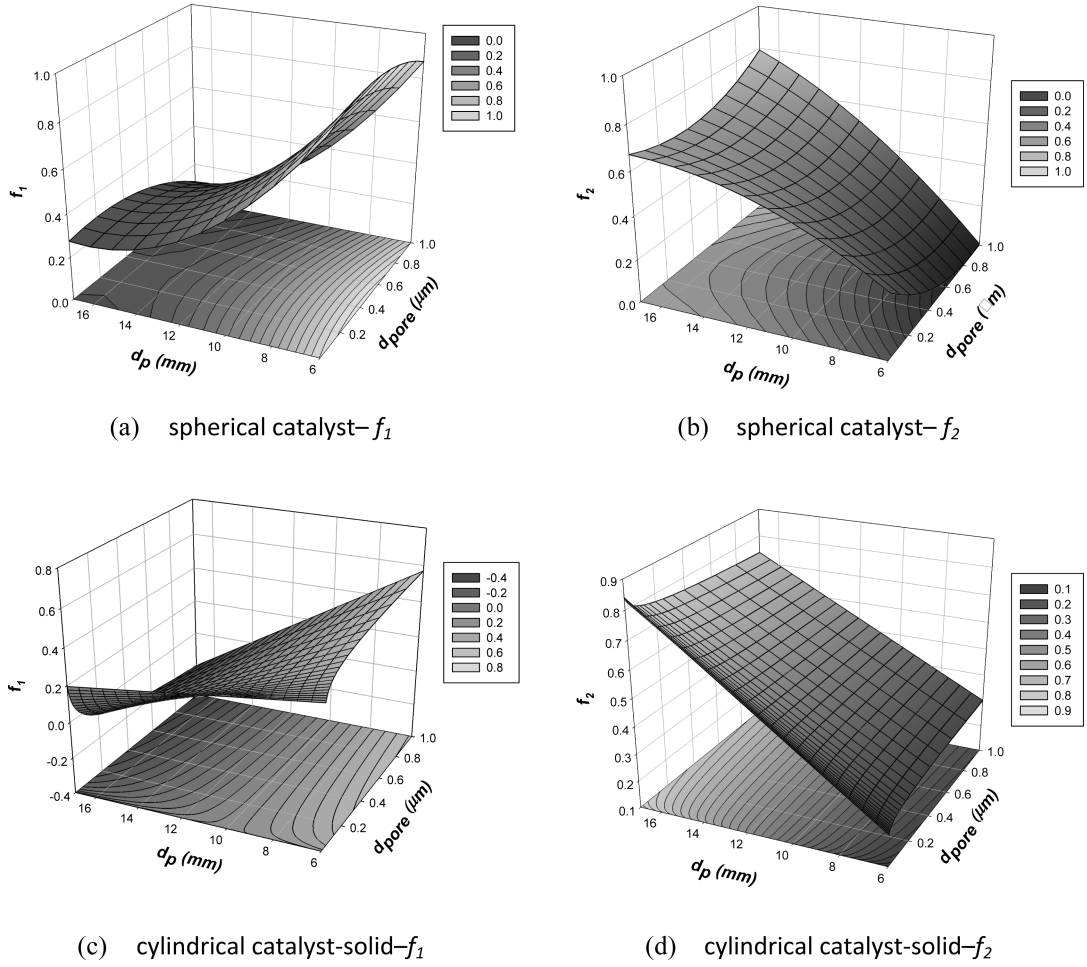

Figure 4. Response surface plots.

Table 4. CFD Simulation Results for Cylindrical Catalyst Design Points

case no.	*Re*	$\Delta P/L$ (Pa/m)	R_1 (10^{-3} kmol/m^3 s)	R_2 (kmol/m^3 s)	ΔR_3 (kmol/m^3 s)	R_4 (kmol/m^3 s)
cylinder-01	25233	15110	2.2947	0.1518	0.4649	0.0764
cylinder-02	7281	28025	3.7429	0.4574	1.4640	0.2439
cylinder-03	11556	29912	3.2389	0.3435	1.0809	0.1770
cylinder-04	13797	14072	3.0841	0.3000	0.9477	0.1522
cylinder-05	17976	17481	2.8711	0.2575	0.8012	0.1304
cylinder-06	13522	12685	3.2454	0.3331	1.0592	0.1725
cylinder-07	16919	24339	2.7366	0.2378	0.7264	0.1190
cylinder-08	11324	15198	3.2637	0.3393	1.0710	0.1727
cylinder-09	8459	56855	3.5709	0.4236	1.3126	0.2233
cylinder-10	10295	16999	3.5127	0.3923	1.2459	0.2058
cylinder-11	14193	30547	3.2226	0.3327	1.0145	0.1717
cylinder-12	7206	26672	3.7569	0.4595	1.4641	0.2449
cylinder-13	18395	9726	3.0788	0.2818	0.8886	0.1442
cylinder-14	14562	9967	3.0076	0.2739	0.8686	0.1377
cylinder-15	23968	16022	2.6470	0.2078	0.6227	0.1045

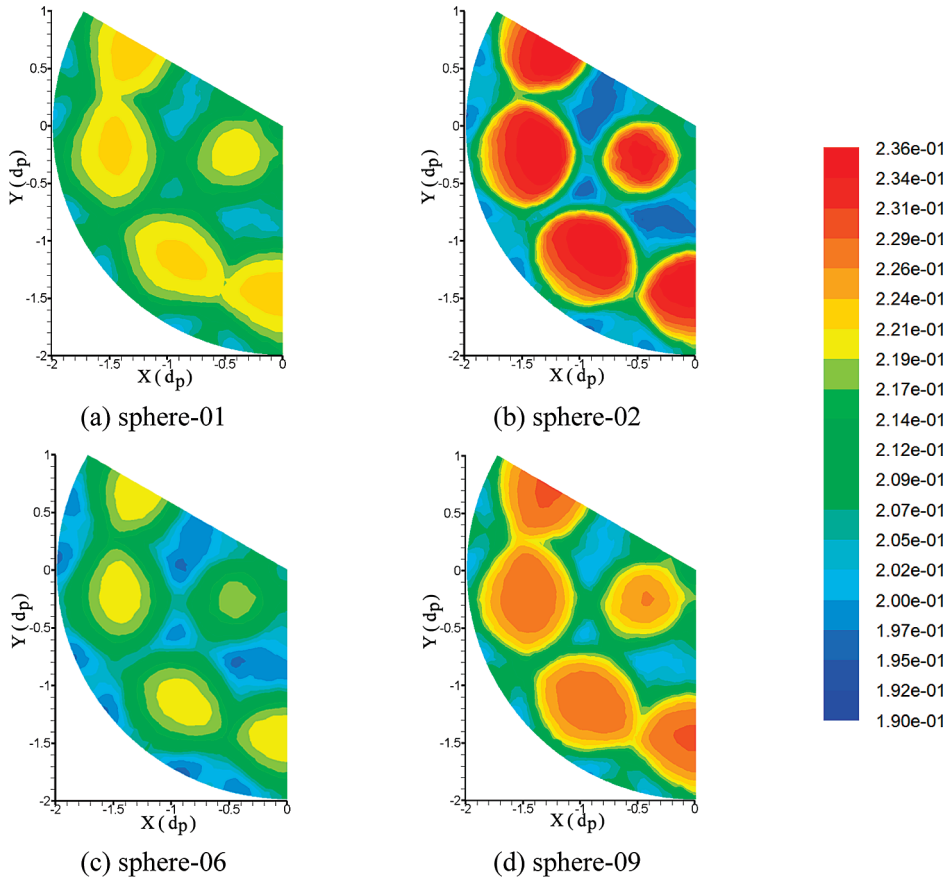

Figure 5. Effects of spherical catalyst pore diameter and particle diameter on H_2 concentration (mole fraction) distribution at the z2 section.

is observable from the intraparticle concentration profile of hydrogen shown in Figure 5. For the catalysts with a smaller pore size, such as 0.018 μm in sphere-02 case, the diffusion is bounded on a thinner surface layer of the particle. With a larger pore size, the concentration variation of the surface layer inside the particle becomes thicker. While comparing the cases with similar particle diameters but very different pore sizes, such as the sphere-01 and sphere-02 cases, the case with a smaller pore

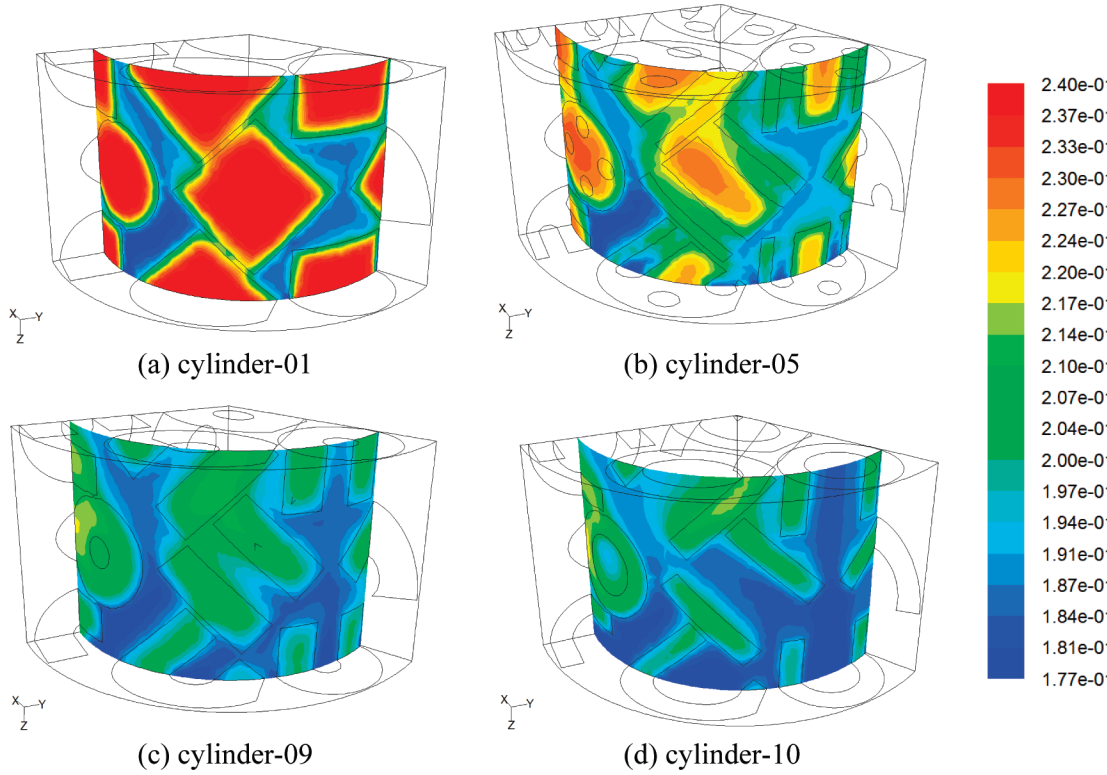

Figure 6. Effects of cylindrical catalyst parameters on H_2 concentration (mole fraction) distribution.

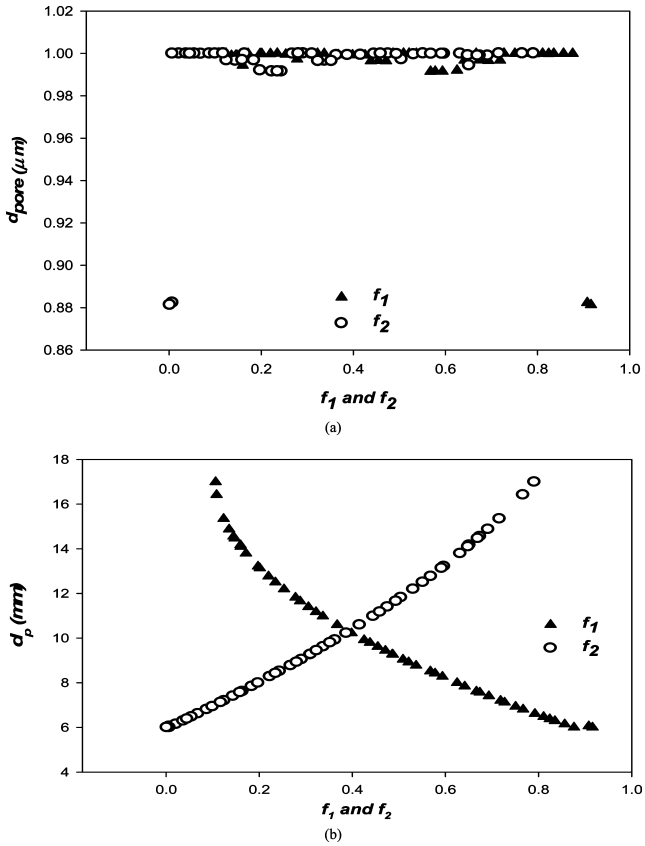

Figure 7. Pareto-optimal solutions for spherical case.

size results in lower reaction rates. The effect of the shape of cylindrical catalysts, namely, the holes of the catalyst pellets, on the hydrogen concentration profile is shown in Figure 6. The fluid concentration distribution is more homogeneous with larger hole sizes or higher voidages.

Optimal Catalyst Design. The multiobjective optimization results are summarized in Figures 7 and 8 for spherical and cylindrical catalysts, respectively. The figures show the distributions of the multiple compromised optimal solutions, 50 solutions, with their values of design variables and objective functions.

For spherical catalysts, the results are as follows:

(1) Except two solutions, which adopt a pore diameter of about 0.88 μm, all other solutions use pore diameters near 1 μm. In the range of study, 0.01−1 μm, large pore diameter is the choice. The reason is that, for both objective functions, the pressure drop and the hydrogen production rate, larger pore size is beneficial.

(2) For the particle diameter, solutions are distributed in the whole study range, i.e., 6−17 mm. The solutions show a continuous trade-off relationship between the hydrogen production rate and the pressure drop.

For cylindrical catalysts, the results are as follows:

(1) For the pore diameter, two groups of solutions are found. The first group uses larger sizes, near 1 μm. The second group uses diameters that fall in the whole study range.

(2) For the particle diameter, the solutions use diameters in two ranges, 6−8 mm or 10−13 mm. The diameters correspond to the catalyst shape of the optimal solutions.

(3) For the catalyst shape, the majority of the solutions use 1-big-hole or 4-hole designs. Only one solution point uses the 4-small-hole shape. For the 4-hole shape design, particle diameters fall in 6−8 mm.

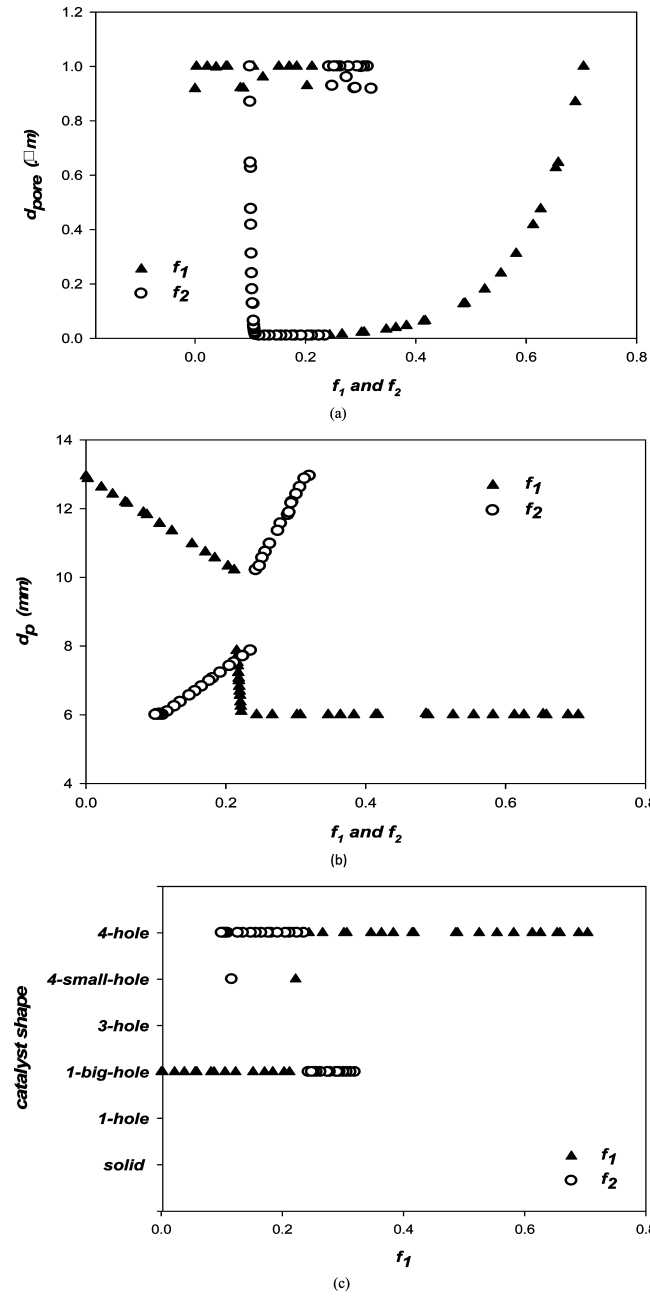

Figure 8. Pareto-optimal solutions for cylindrical case.

On the other hand, the 1-big-hole shape design uses larger particle diameter, 10−13 mm, and the pore sizes are larger too, near 1 μm.

Conclusions

Although CFD simulation is expensive in computation and is difficult to directly apply for optimization, this work has demonstrated the utilization of CFD simulation for the catalyst design of a methane steam reforming packed bed reactor employing spherical or cylindrical catalysts with a tube-to-particle diameter ratio (N) of 4. The integrated optimization approach adopted incorporates CFD simulation with a Latin hypercube design, a response surface method, and the NSGA-II genetic algorithm.

With the binary objective functions, pressure drop and hydrogen production rate, and the given inlet gas conditions, the optimal solutions for catalyst design are (1) spheres with a large pore size near 1 μm, (2) 1-big-hole cylinders with a particle diameter of 10−13 mm and a pore size near 1 μm, or (3) 4-hole cylinders with a particle diameter of 6−8 mm.

Acknowledgment

The authors thank the funding from the National Science Council of Taiwan.

Nomenclature

C_p = heat capacity at constant pressure, J kg^{-1} K^{-1}
d = number of variables
D_i = molecular diffusivity of species i, m^2 s^{-1}
d_P = diameter of catalyst particle, m
d_{pore} = pore diameter of catalyst, m
f_i = objective function i
$\vec{F}$ = force vector, N
h_i = enthalpy of species i, J kg^{-1}
h_i^o = formation enthalpy of species i, J kg^{-1}
I = unit tensor
J_i = diffusion flux of species i, kg/m^2 s
k = turbulent kinetic energy, m^2 s^{-2}
k_c = thermal conductivity, W m^{-1} K^{-1}
L = reactor length, m
M_w = molecular weight
N = tube-to-particle diameter ratio
P = pressure, kg m^{-1} s^{-2}
ΔP = pressure drop, kg m^{-1} s^{-2}
Pr_t = turbulent Prandtl number
R_i = reaction rate of reaction i, kmol m^{-3} s^{-1} or kg m^{-3} s^{-1}
$\hat{R}_{i,r}$ = Arrhenius molar rate of creation/destruction of species i in reaction r, kmol m^{-3} s^{-1}
R^2 = coefficient of determination
Re = Reynolds number
Sc_t = turbulent Schmidt number
S_h = volumetric heat source, J m^{-3} s^{-1}
$\vec{v}$ = velocity vector, m s^{-1}
x = design variable
y_i = mass fraction of species i
y^+ = dimensionless distance parameter

Greek Letters

α = permeability, m^2
α_i = regression coefficient i
β = regression coefficient
ε = total error
ϵ = turbulent dissipation rate, m^2 s^{-3}
μ = viscosity, kg m^{-1} s^{-1}
μ_t = turbulent viscosity, kg m^{-1} s^{-1}
ρ = density, kg m^{-3}
$\bar{\tau}$ = stress tensor, Pa

Subscripts

adj = adjusted
ref = reference

Literature Cited

(1) Twigg, M. *Catalyst Handbook*, 2nd ed.; Wolfe Publishers: London, UK, 1997.

(2) Dixon, A. G.; Nijemeisland, M.; Stitt, E. H. Packed Tubular Reactor Modeling and Catalyst Design Using Computational Fluid Dynamics. In *Advances in Chemical Engineering 31*; Marin, G. B., Ed.; Academic Press: San Diego, CA, 2006; pp 308−390.

(3) Dixon, A. G. Heat Transfer in Fixed Beds at Very Low (<4) Tube-to-Particle Diameter Ratio. *Ind. Eng. Chem. Res.* **1997**, *36*, 3053–3064.

(4) Romkes, S. J. P.; Dautzenberg, F. M.; van den Bleek, C. M.; Calis, H. P. A. CFD Modelling and Experimental Validation of Particle-to-Fluid Mass and Heat Transfer in a Packed Bed at Very Low Channel to Particle Diameter Ratio. *Chem. Eng. J.* **2003**, *96*, 3–13.

(5) Guardo, A.; Coussirat, M.; Larrayoz, M. A.; Recasens, F.; Egusquiza, E. CFD Flow and Heat Transfer in Nonregular Packings for Fixed Bed Equipment Design. *Ind. Eng. Chem. Res.* **2004**, *43*, 7049–7056.

(6) Nijemeisland, M.; Dixon, A. G. CFD Study of Fluid Flow and Wall Heat Transfer in a Fixed Bed of Spheres. *AIChE J.* **2004**, *50*, 906–921.

(7) Gunjal, P. R.; Ranade, V. V.; Chaudhari, R. V. Computational Study of a Single-Phase Flow in Packed Beds of Spheres. *AIChE J.* **2005**, *51*, 365–378.

(8) Dixon, A. G.; Taskin, M. E.; Stitt, E. H.; Nijemeisland, M. 3D CFD Simulations of Steam Reforming with Resolved Intraparticle Reaction and Gradients. *Chem. Eng. Sci.* **2007**, *62*, 4963–4966.

(9) Dixon, A. G.; Nijemeisl, M.; Stitt, H. CFD Simulation of Reaction and Heat Transfer Near the Wall of a Fixed Bed. *Int. J. Chem. Reactor Eng.* **2003**, *1*, A22.

(10) Nijemeisland, M.; Dixon, A. G.; Stitt, E. H. Catalyst Design by CFD for Heat Transfer and Reaction in Steam Reforming. *Chem. Eng. Sci.* **2004**, *59*, 5185–5191.

(11) Taskin, M. E.; Dixon, A. G.; Nijemeisland, M.; Stitt, E. H. CFD Study of the Influence of Catalyst Particle Design on Steam Reforming Reaction Heat Effects in Narrow Packed Tubes. *Ind. Eng. Chem. Res.* **2008**, *47*, 5966–5975.

(12) Deb, K. *Multi-Objective Optimization Using Evolutionary Algorithms*; John Wiley and Sons, Ltd.: New York, 2001.

(13) Rajesh, J. K.; Gupta, S. K.; Rangaiah, G. P.; Ray, A. K. Multiobjective Optimization of Steam Reformer Performance using Genetic Algorithm. *Ind. Eng. Chem. Res.* **2000**, *39*, 706–717.

(14) Kasat, R. B.; Kunzru, D.; Saraf, D. N.; Gupta, S. K. Multiobjective Optimization of Industrial FCC Units using Elitist Nondominated Sorting Genetic Algorithm. *Ind. Eng. Chem. Res.* **2002**, *41*, 4765–4776.

(15) Chang, H.; Hou, W.-C. Optimization of Membrane Gas Separation Systems using Genetic Algorithm. *Chem. Eng. Sci.* **2006**, *61*, 5355–5368.

(16) Cheng, S.-H.; Chen, H.-J.; Chang, H.; Chang, C.-K.; Chen, Y.-M. Multi-objective Optimization for Two Catalytic Membrane Reactors - Methanol Synthesis and Hydrogen Production. *Chem. Eng. Sci.* **2008**, *63*, 1428–1437.

(17) Lian, Y.; Liou, M.-S. Multiobjective Optimization Using Coupled Response Surface Model and Evolutionary Algorithm. *AIAA J.* **2005**, *43*, 1316–1325.

(18) Yu, Y.-H. Simulation of Secondary Reformer in Industrial Ammonia Plant. *Chem. Eng. Technol.* **2002**, *25*, 307–314.

(19) De Groote, A. M.; Froment, G. F. Simulation of the Catalytic Partial Oxidation of Methane to Synthesis Gas. *Appl. Catal., A* **1996**, *138*, 245–264.

(20) Xu, J.; Froment, G. F. Methane Steam Reforming, Methanation and Water-gas Shift: I. Intrinsic Kinetics. *AIChE J.* **1989**, *35*, 88–96.

(21) Dixon, A. G.; Nijemeisland, M.; Stitt, E. H. CFD Study of Heat Transfer near and at the Wall of a Fixed Bed Reactor Tube: Effect of Wall Conduction. *Ind. Eng. Chem. Res.* **2005**, *44*, 6342–6353.

(22) *FLUENT 6.3 User's Guide*; Fluent Inc.: Lebanon, NH, 2006.

(23) Ergun, S. Fluid Flow Through Packed Columns. *Chem. Eng. Prog.* **1952**, *48*, 89–94.

(24) Calis, H. P. A.; Nijenhuis, J.; Paikert, B. C.; Dautzenberg, F. M.; van den Bleek, C. M. CFD Modeling and Experimental Validation of Pressure Drop and Flow Profile in a Novel Structured Catalytic Reactor Packing. *Chem. Eng. Sci.* **2001**, *56*, 1713–1720.

(25) Buffham, B. A. Design Relations for Hollow Catalyst Pellets. *AM Trans IChemE A* **2000**, *78*, 269–282.

(26) Afandizadeh, S.; Foumeny, E. A. Design of Packed Bed Reactors: Guides to Catalyst Shape, Size, and Loading Selection. *Appl. Therm. Eng.* **2001**, *21*, 669–682.

(27) Bartholomew, C. H.; Farrauto, R. J. *Fundamentals of Industrial Catalytic Processes*, 2nd ed.; Wiley: New York, 2006.

(28) Myers, R. H.; Montgomery, D. C. *Response Surface Methodology: Process and Product Optimization using Designed Experiments*; John Wiley & Sons, Inc.: New York, 1995.

(29) McKay, M. D.; Beckman, R. J.; Conover, W. J. A Comparison of Three Methods for Selecting Values of Input Variables in the Analysis of Output from a Computer Code. *Technometrics* **1979**, *21*, 239–245.

(30) Unal, R.; Lepsch, R. A.; McMillin, M. L. Response Surface Model Building and Multidisciplinary Optimization Using D-Optimal Design. *AIAA J.* **1998**, 98–4759.

(31) Deb, K.; Patap, A.; Agrawal, S.; Meyarivan, T. A. Fast and Elitist Multiobjective Genetic Algorithm: NSGA-II. *IEEE Trans. Evol. Comput.* **2002**, *6*, 182–197.

Received for review January 26, 2010
Revised manuscript received April 16, 2010
Accepted April 21, 2010

IE1001839